

General Method of Manipulating Formation, Composition, and Morphology of Solid-Electrolyte Interphases for Stable Li-Alloy Anodes

Yue Gao,[‡] Ran Yi,[†] Yuguang C. Li,[‡] Jiangxuan Song,^{†,§} Shuru Chen,[†] Qingquan Huang,[†] Thomas E. Mallouk,[‡] and Donghai Wang^{*,†}

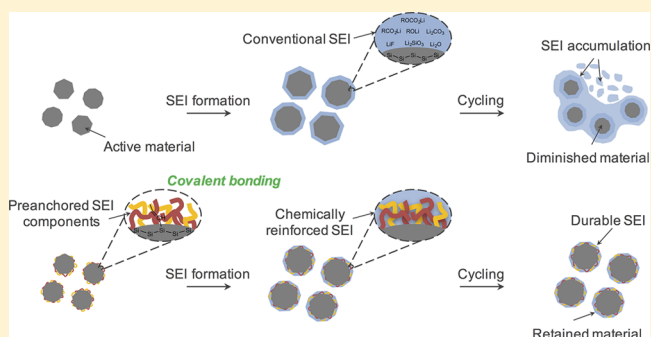
[†]Department of Mechanical and Nuclear Engineering, The Pennsylvania State University, University Park, Pennsylvania 16802, United States

[‡]Department of Chemistry, The Pennsylvania State University, University Park, Pennsylvania 16802, United States

[§]State Key Laboratory for Mechanical Behavior of Materials, Xi'an Jiaotong University, Xi'an 710049, China

Supporting Information

ABSTRACT: Li-alloy-based anode materials are very promising for breaking current energy limits of lithium-ion battery technologies. Unfortunately, these materials still suffer from poor solid-electrolyte interphase (SEI) stability, resulting in unsatisfied electrochemical performances. The typical SEI formation method, electrochemical decomposition of electrolytes onto the active material surface, lacks a deliberate control of the SEI functions and structures. Here we propose a general method of manipulating the formation process, chemical composition, and morphology of the SEI for Li-alloy anodes, using Si and Ge nanoparticle anodes as the platform. The SEI was fabricated through a covalent anchoring of multiple functional components onto the active material surface, followed by electrochemical decomposition of the functional components and conventional electrolyte. Click reaction, serving as the covalent anchoring approach, allows an accurate control of the SEI composition and structure at the molecular level through tuning the chemical structure and amount of variety of functional components and provides an intimate contact between the SEI and the Li-alloy material surface contributed by the covalent bonding. The optimized Si nanoparticle SEI, functionalized by a unique combination of diverse components and containing a high concentration of organic components attributed to the preanchored functional components, presented a stable composition and durable morphology during cycling and led to an improved first cycle efficiency of Si nanoparticle anodes and its long cycle life in a full cell. This general method displays potential benefits to construct stable SEIs for other Li-alloy anodes.



INTRODUCTION

Li-alloy-based anode materials from group IV (Si, Ge, etc.) and group V (P, Sb, etc.) are some of the most promising anode candidates for next-generation Li-ion batteries (LIBs), with capacities several times greater than that of the conventional graphite anode.^{1–5} These materials undergo a huge volume change and pulverization and more importantly present poor stability of the solid-electrolyte interphase (SEI) during lithiation–delithiation.^{6,7} Despite considerable efforts on advanced material designs of nanostructures,^{8–13} composites,^{14–16} and functional polymer incorporation^{17,18} to address issues resulting from volume changes, the poor stability of the SEI is still a major obstacle to achieving the desired electrochemical performance of Li-alloy anodes. The typical SEI, generated from electrolyte decomposition, presents not only insufficient integrity and a weak contact with active material surface, resulting in cracking and peeling-off issues during volume changes, but also a less efficient surface passivation, causing the electrolyte penetration (Figure 1a).

These facts occurring in each cycle consume additional electrolyte and material for the SEI repair and cause a poor electrochemical performance of the anode.^{19–27}

Two general strategies have been developed to address SEI stability issues. One is to insert a protective layer between Li alloy anodes and the electrolyte, either serving as an artificial SEI^{28–33} or forming a stable SEI on the protective layer surface,^{34–38} circumventing the undesired SEI chemistry of Li-alloy anodes. During repeated volume changes upon cycling, it is still challenging to sufficiently protect Li-alloy anode materials from reactions with the electrolyte due to electrolyte penetration from cracks and defects in the protective layers. The second strategy is to optimize SEI compositions of Li-alloy anode materials by tuning the electrolytes, including Li salts,^{39,40} aprotic solvents,⁴¹ and additives.^{39,42–45} Despite improvements in the flexibility and surface passivation of the

Received: July 20, 2017

Published: October 30, 2017

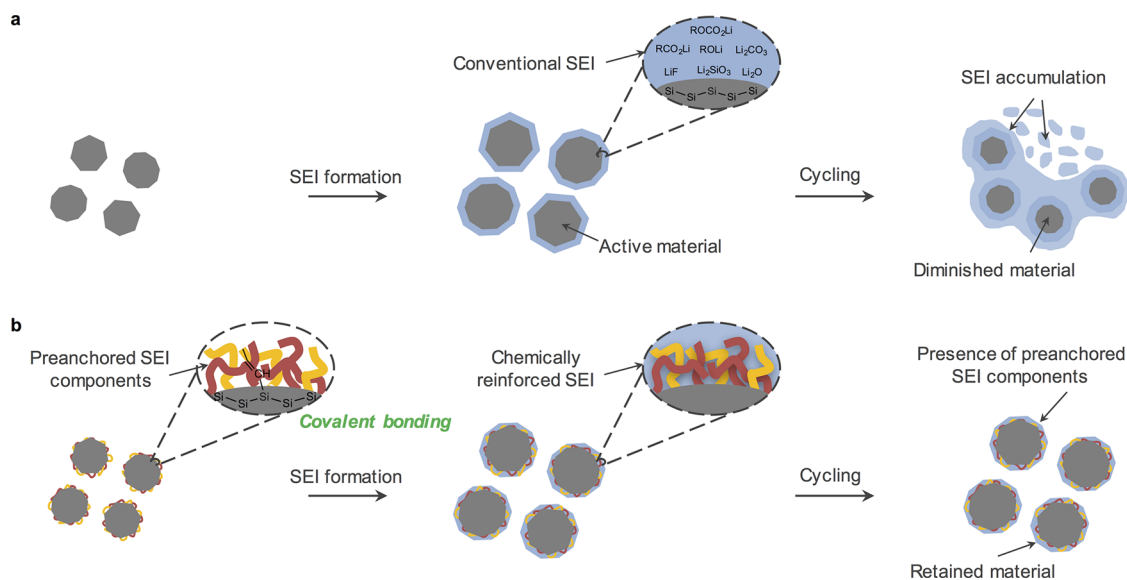


Figure 1. Schematic illustration of the CR-SEI. (a) A conventional SEI contains high-concentration inorganic Li salts and presents weak interactions with electrode material surface, showing poor tolerance to the volume change and insufficient surface passivation. During cycling, it breaks and loses contact with the electrode material surface, resulting in severe consumption of electrode material and electrolyte and accumulation of “waste SEI”. (b) The CR-SEI, reinforced by diverse preanchored SEI components, with high-concentration organic oligomers and covalent bonding interactions (e.g., Si–C bonds) with the electrode material surface, presents good stability during cycling. Pristine SiNP was first anchored with multiple functional components (red and yellow lines) and used for electrode and cell fabrication. At the first lithiation, the CR-SEI was *in situ* formed, composed of the preanchored components after electrochemical activation and conventional SEI components (blue) from electrolyte decomposition.

SEI, the SEI peeling-off issue remains unsolved. More importantly, the current technologies are not able to deliberately control the SEI composition and structure with desired properties. It is desirable to develop an approach capable of designing and controlling the SEI to understand composition–structure–property relationships of the SEI and direct further SEI optimization.

We herein propose a general SEI reinforcement strategy for Li-alloy-based anode materials (Figure 1b), one manipulating the SEI formation process and chemical composition using a combination of diverse functional components to reinforce its stability during cycling. The altered SEI formation process contains two steps. First, a variety of functional components were one-step covalently anchored onto the Li-alloy material surface with precisely controlled structure and amount via a click reaction. Second, these preanchored components were electrochemically activated along with the electrolyte decomposition, forming a chemically reinforced SEI (CR-SEI). The CR-SEI presents reinforced tolerance to volume changes and enhanced surface passivation, owing to the addition of the preanchored components. Also, the covalent bonding between the preanchored components and the Li-alloy material surface provides a durable contact between the SEI and the active material surface.

A Si nanoparticle (SiNP) material was employed as a platform to demonstrate the CR-SEI concept because it has a very high specific capacity and presents severe SEI issues, which presents a poor electrochemical performance when using SiNP-only fabricated anodes.^{4,7} A variety of single components and their combinations were covalently bonded onto the SiNPs to investigate their effects on SEI reinforcement. Among those components, an SEI reinforced by a combination of two organic oligomer components with a moderate anchoring amount presents the most optimized SEI stability. Unlike the

conventional SEI, the CR-SEI is a thin layer intimately contacted to the SiNP surface that contains extensively increased concentrations of organic species, contributed by the preanchored functional components. Owing to these reinforced characteristics, it exhibits a durable chemical composition and morphology during cycling. Compared to SiNP electrodes with electrolyte additives, SiNP-only fabricated electrodes with a CR-SEI in the absence of any electrolyte additives show significantly improved electrochemical performance, including increased first cycle Coulombic efficiency (CE), improved cycling CE and capacity retention, and limited increase in electrochemical impedance. This strategy was applied to the SEI reinforcement of Ge nanoparticle materials (GeNP), and significantly increased stability was also achieved, verifying its applicability to other Li-alloy materials.

RESULTS AND DISCUSSION

Structural Screening and Optimization of the CR-SEI.

Diverse preanchored components including four individual compounds and their combinations have been prepared for SEI reinforcement (Figure 2a). 2' (*O*-(2-azidoethyl)-*O*-methyl undecaethylene glycol) and 3' (*O*-(2-azidoethyl)-*O*-methyl triethylene glycol), containing the repeating unit of ethylene oxide with different lengths, were designed as organic oligomers. 4' (4-azidomethyl-5-methyl-1,3-dioxol-2-one) and 5' (4-azido-5-fluoro-1,3-dioxolan-2-one) were designed as analogues of vinylene carbonate (VC) and fluoroethylene carbonate (FEC). Combinations of 2'–4' and 3'–4' were designed to functionalize the SEI synergistically.

All SiNPs with various preanchored components with different anchoring amounts were synthesized via Cu(I)-catalyzed click reaction (Figures 2a, S1). Briefly, preanchored components and SiNPs were first modified with azide and alkyne end groups, respectively, and then covalently bonded

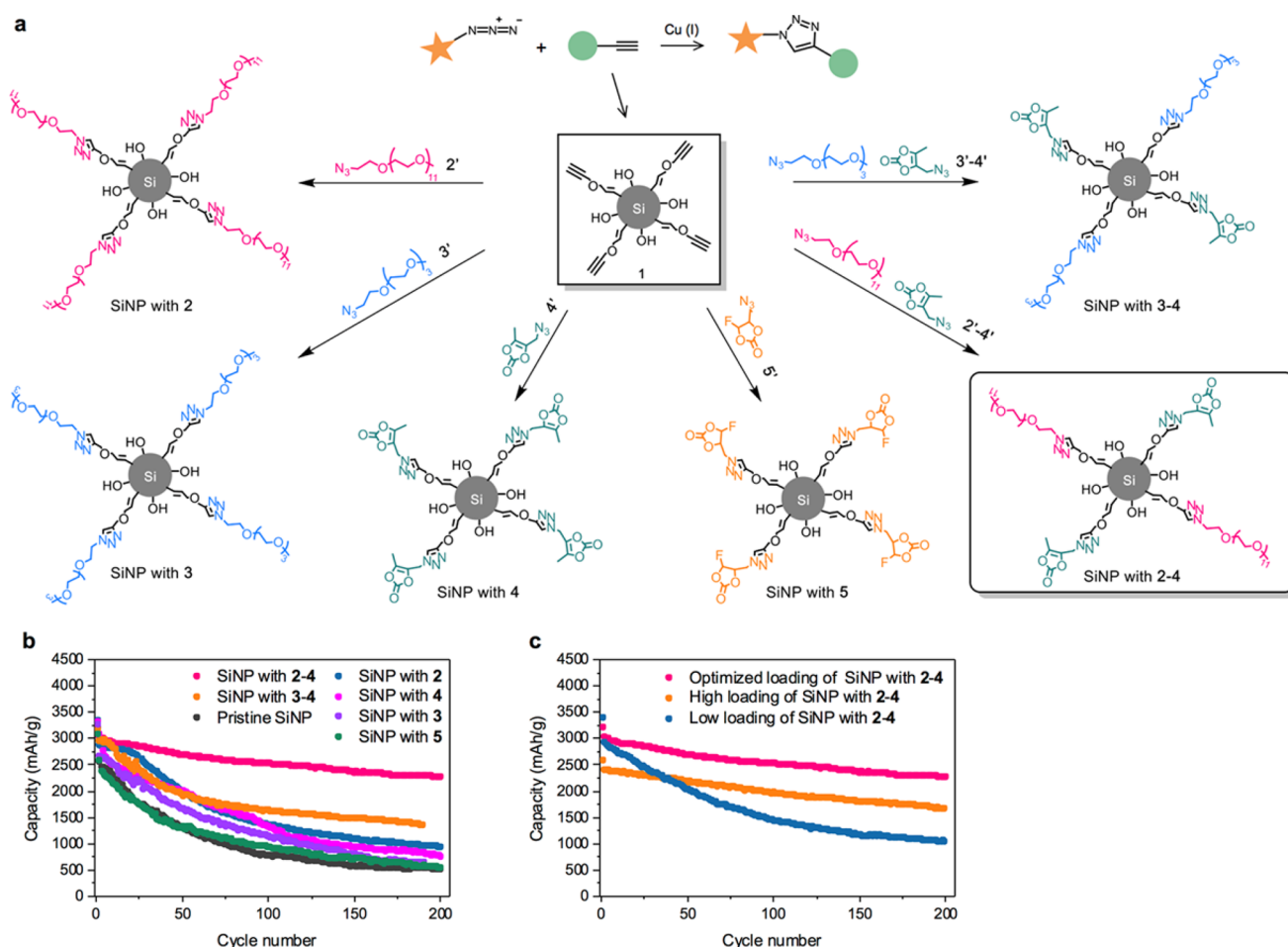


Figure 2. Structural design and screening of the chemically reinforced SEI. (a) Structural design and synthesis of SiNPs with various functional preanchored components. All these materials were prepared by the modular and high-efficiency click reaction. (b) Structural optimization of SiNP with preanchored components depicted in a half-cell cycling performance measurement. The combination of 2'–4' (in the highlighted box) shows a better performance. (c) Optimization of the anchoring amount of SiNP with 2–4 through half-cell testing. The SiNP with the optimized loading of 2' and 4' exhibits the best cycling stability (pink line in b and c).

together via a triazole linker. This high-efficiency reaction has no selectivity to the structures of both material and preanchored components, presents nearly 100% yield, and is conducted under mild conditions without byproduct formation.^{46,47} These advantages enable the strategy to serve as a facial and general approach for SEI construction and optimization of Li-alloy anodes. The syntheses were verified by NMR, X-ray photoelectron spectroscopy (XPS), Fourier-transform infrared spectra (FTIR), and thermal gravimetric analysis (TGA) (Figure S2).

The screening and optimization of these components were carried out based on their half-cell performances. First, the effects of different functional components were investigated (Figure 2b). The addition of 2, 3, 4, 2–4, or 3–4 improves the cycling performance of SiNP anodes, implying the enhancement of SEI stability. Interestingly, the combination of 2–4 or 3–4 shows better cycling performance than any single component, indicating the benefits of multifunctionalizing the SEI. Second, we studied the effects of different anchoring amounts of the combination of 2–4. As shown in Figure 2c, SiNPs with a molar ratio of SiNP:2':4' = 100:1:1.5 exhibit the most optimized cycling performance. SiNPs with a lower anchoring amount of 2–4 (SiNP:2':4' = 100:0.5:0.5) show faster capacity fading, indicating an insufficient functionalization

of the SEI. The higher anchoring SiNPs (Si:2':4' = 100:2.5:2.5) present a decreased specific capacity but a good cyclability, since the high loading of preanchored components may have lowered the electrical conductivity of the entire SEI.

Finally, the CR-SEI reinforced by 2–4 with a moderate anchoring amount was used for further analysis. In this CR-SEI, 2 containing ethylene oxide chains has strong noncovalent interactions with conventional SEI components such as lithium vinylene carbonate (ROCO₂Li), lithium carbonate (Li₂CO₃), and lithium oxide (Li₂O) and enhances the flexibility of the entire SEI.⁴⁸ 4 is electrochemically activated *in situ* and forms oligomeric species with the electrolyte, and thus improves the surface passivation of the SEI. Meanwhile, the covalent bonding between both preanchored components and the SiNP surface allows the CR-SEI to have intimate contact with the SiNP electrode surface during cycling.

Electrochemical Characterization of CR-SEI. To investigate the reinforcing effects of the CR-SEI, we next evaluated the electrochemical performance of SiNP electrodes with the CR-SEI in the absence of any electrolyte additives and compared it with the performance of SiNP electrodes containing conventional electrolyte-derived SEI (conventional SEI) and a conventional electrolyte with a fluoroethylene carbonate additive-derived SEI (FEC-SEI).

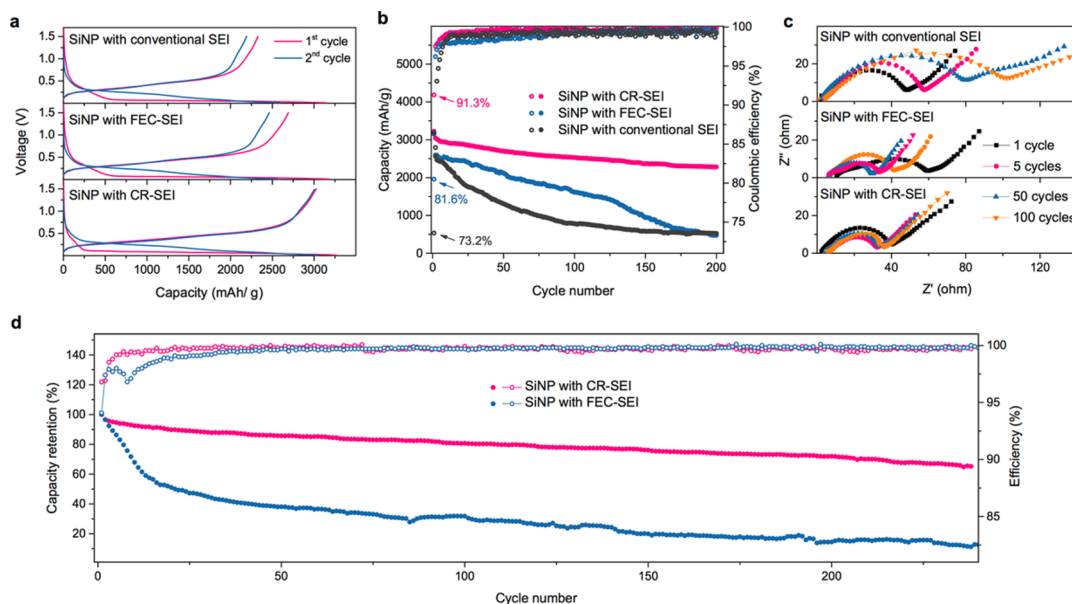


Figure 3. Electrochemical performance of SiNPs with the chemically reinforced SEI. (a) Voltage profile and SEI formation of SiNP electrodes with a CR-SEI, FEC-SEI, and conventional SEI during initial cycles. The SiNP electrode with a CR-SEI shows a much lower capacity related to SEI formation, implying the decreased consumption of electrode and electrolyte materials. (b) Specific capacities and Coulombic efficiencies (CE) of SiNP electrodes with a CR-SEI (pink), FEC-SEI (blue), and conventional SEI (gray) in half-cells. Compared with a SiNP electrode with an FEC-SEI or conventional SEI, a SiNP electrode with a CR-SEI presents greatly improved cycling life and cycling CE, indicating its benefits to cycling performance. The significantly increased first cycle CE of a SiNP electrode with a CR-SEI also indicates the decreased consumption of electrolyte and material by SEI formation, consistent with the findings in a. (c) EIS measurements of SiNP electrodes with a conventional SEI, FEC-SEI, and CR-SEI after different cycling. The resistance of a SiNP electrode with a CR-SEI increases quite slowly, indicating limited SEI accumulation and good stability during cycling. (d) Full-cell capacity retention and CE of SiNP electrodes with a CR-SEI (pink) and FEC-SEI (blue), paired with a $\text{LiNi}_{0.5}\text{Co}_{0.2}\text{Mn}_{0.3}\text{O}_2$ cathode. A SiNP electrode with a CR-SEI delivers dramatically improved capacity retention and CE, compared with a SiNP electrode with an FEC-SEI, resulting from its enhanced SEI stability, especially the decreased consumption of Li source during cycling.

During the first lithiation, SiNP electrodes with the CR-SEI show a capacity of about 280 mAh/g in the voltage range of 1 to 0.1 V (Figure 3a), which is mainly due to initial SEI formation. In contrast, the capacities for forming the conventional SEI and FEC-SEI in SiNP electrodes are 515 and 523 mAh/g (Figure 3a), respectively. This result indicates much less consumption of electrolyte and electrode material for CR-SEI formation. This result is consistent with the increased first cycle efficiency to 91.3% in SiNP with CR-SEI, compared to 73.2% for a conventional SEI and 81.6% for the FEC-SEI (Figure 3b). In addition, the SiNP electrode with CR-SEI presents significantly improved cycling stability with a specific capacity of 2280 mAh/g for up to 200 cycles and a high cycling CE of 99.6% in 200 cycles (Figure 3b). This is in dramatic contrast with the FEC-SEI and conventional SEI, which only deliver specific capacities of 1613 and 784 mAh/g after 100 cycles and CEs of 98.5% and 97.3%, respectively (Figure 3b). Meanwhile, the CE of the SiNP electrode with the CR-SEI reaches 99% in the ninth cycle and maintains this level afterward, indicating the accelerated formation of a stable SEI (Figure 3b). Furthermore, electrochemical impedance spectroscopy (EIS) measurements of a SiNP electrode after different cycles were also monitored. The overall charge transfer resistances of SiNP electrodes with a CR-SEI are quite low and remain stable during cycling, in contrast to the continuously increasing resistances of electrodes with both SiNP with FEC-SEI and a conventional SEI (Figure 3c). Finally, we evaluated full-cell performances using the SiNP only as the anode paired with a commercial $\text{LiNi}_{0.5}\text{Co}_{0.2}\text{Mn}_{0.3}\text{O}_2$ cathode to further verify the stability of the CR-SEI. As shown in Figure 3d, the full cell displays discharge capacity retentions of 90.2%, 83.0%, and 72.0% after 20, 80, and

200 cycles, respectively, and a high average CE of 99.7% during 240 cycles. This is much better than the performance of SiNPs with an FEC-SEI, which exhibits discharge capacity retentions of 50.5%, 29.5%, and 13.8% after 20, 80, and 200 cycles, respectively, and a low CE of 98.7% in 50 cycles. As the Li source in the full-cell system is limited, the significantly improved cycling life and CE of the full cell using the SiNP CR-SEI demonstrates a dramatic enhancement of the CR-SEI stability and the suppressed Li consumption during cycling. Overall, these improvements in electrochemical performance strongly verify the effective reinforcement of the preanchored components that leads to SEI stability. Since a pure SiNP electrode with high areal capacity faces very extreme SEI issues, this is one of the best cycling performances, as far as we are aware.

We also applied this optimized CR-SEI to a GeNP anode, another promising Li-alloy anode. Following a similar synthetic approach, a GeNP with 2–4 was synthesized (Figure S4). A GeNP anode with the CR-SEI exhibits greatly enhanced cycling performance and CE compared with GeNPs with an FEC-SEI and a conventional SEI (Figure S5).

Compositional Analysis of the CR-SEI. To study the reinforcement mechanism of the preanchored components to the CR-SEI, we analyzed the chemical composition and compositional evolution of a CR-SEI during cycling. High-resolution XPS measurements of both a cycled SiNP electrode with a CR-SEI and a SiNP electrode with a conventional SEI reveal clear differences in their chemical compositions because of the presence/absence of preanchored SEI components (Figure 4a). The conventional SEI shows peaks at 289.2 and 282.3 eV attributed to C=O and R–Li, respectively, in the C

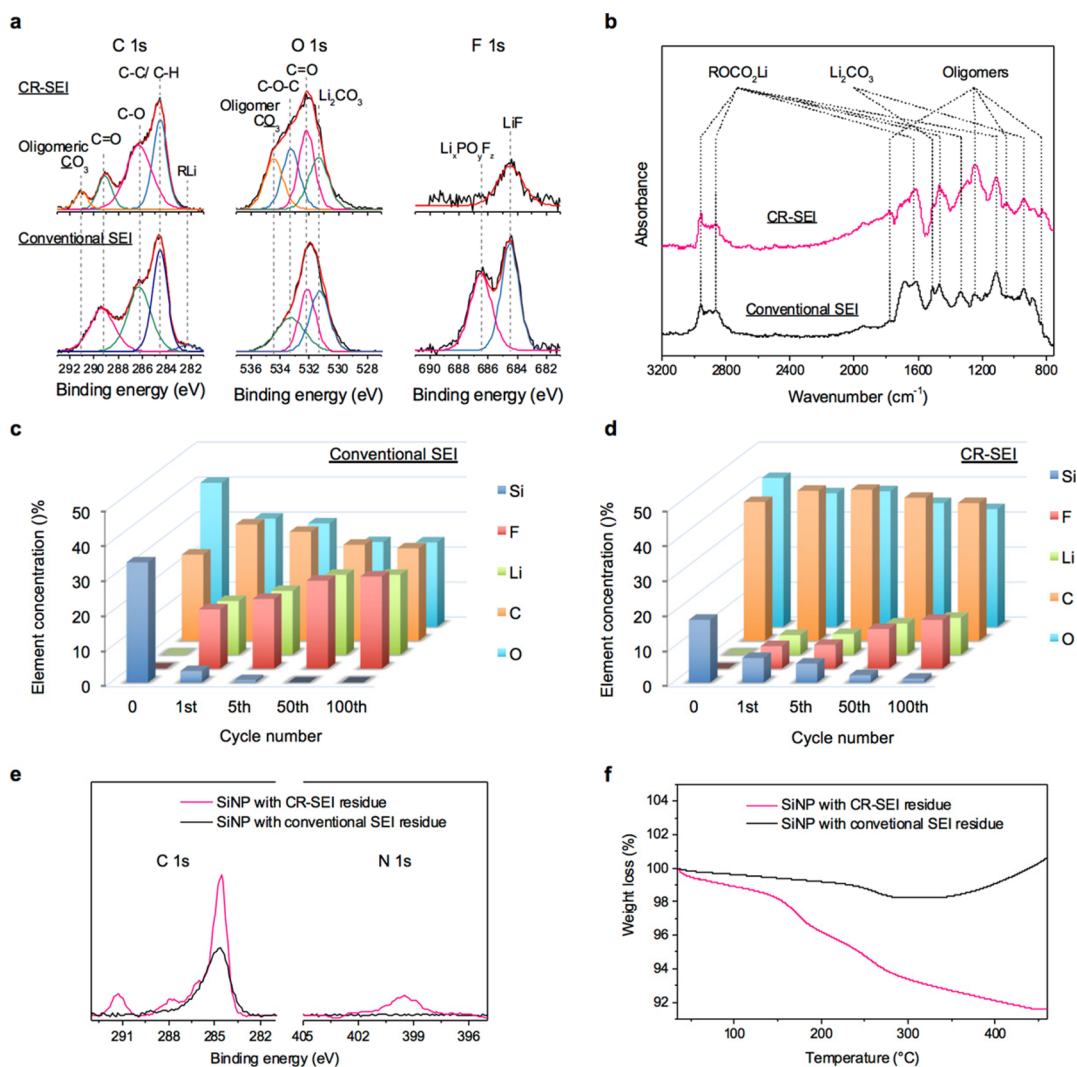


Figure 4. Compositional analysis of a CR-SEI. High-resolution XPS spectra (a) and FTIR analysis (b) of a SiNP with a CR-SEI (top) and a SiNP with a conventional SEI (bottom) after 30 cycles. Compared with a conventional SEI, newly appearing peaks in the spectra of a SiNP with a CR-SEI are assigned to the increased concentrations of the organic and oligomeric species in the chemically reinforced SEI, demonstrating the presence of the preanchored components in the SEI. Elemental concentration analysis of a conventional SEI (c) and a CR-SEI (d) after different cycles. This trend analysis of the concentrations of C, O, Li, F, P, and Si in the SEI reveals that the CR-SEI contains significantly increased organic species and its composition remains stable during cycling. High-resolution XPS spectra (e) and TGA (f) of the Si with a CR-SEI residue (pink) and Si with a conventional SEI residue (black). After removing the SEI by the wash and ultrasonic treatment, the Si with a CR-SEI presents the characteristic signals of preanchored components in the XPS spectrum and 8% weight loss below 450 °C, both indicating the durable bonding of preanchored components on an electrode material surface.

1s spectrum, peaks at 532.2 and 531.2 eV corresponding to C=O and Li_2CO_3 , respectively, in the O 1s spectrum, and peaks at 686.5 and 684.5 eV assigned to $\text{Li}_x\text{PO}_y\text{F}_z$ and LiF, respectively, in the F 1s spectrum. This result is consistent with previous studies of SEI compositions using carbonate-based electrolytes.^{21,49,50} As for the CR-SEI, new peaks appeared at 291.1 and 534.5 eV belonging to the oligomeric species of 4.^{39,48} The concentrations of C–O in both C 1s and O 1s spectra are considerably increased, caused by the addition of both the ethylene oxide repeating unit from 2 and the C–O from 4. This result clearly affirms the introduction of the covalently bonded components into the CR-SEI. Additionally, the concentration of LiF is quite low and the $\text{Li}_x\text{PO}_y\text{F}_z$ signal is negligible, implying that LiPF_6 decomposition is limited due to the effective surface passivation of the CR-SEI.⁴⁸ FTIR results are consistent with the findings from high-resolution XPS measurements (Figure 4b). Spectra of a SiNP electrode with a

CR-SEI and a SiNP electrode with a conventional SEI electrode both display peaks from electrolyte-decomposed products, including ROCO_2Li with peaks at 2959 and 2865 cm^{-1} ($\nu\text{C–H}$), 1624 cm^{-1} ($\nu\text{C=O}$), 1462 cm^{-1} ($\delta\text{C–H}$), 1332 cm^{-1} ($\nu\text{C=O}$), and 1108 cm^{-1} ($\nu\text{C–O}$) and Li_2CO_3 with peaks at 1509 and 941 cm^{-1} . Notably, the peaks at 1775, 1249, 1050, and 831 cm^{-1} in the spectra of the SiNP electrode with a CR-SEI are assigned to the organic oligomeric species,⁴⁹ which are absent in the spectrum of the SiNP electrode with a conventional SEI, suggesting the presence of preanchored components in the CR-SEI.

Apart from compositional analysis, the compositional evolution during cycling provides useful information on SEI stability. XPS elemental analysis of the SiNP electrodes after 0, 1, 5, 50, and 100 cycles was carried out. In the LiPF_6 /carbonate electrolyte system, Li and F concentrations in the SEI are related to the amount of decomposed LiPF_6 species.

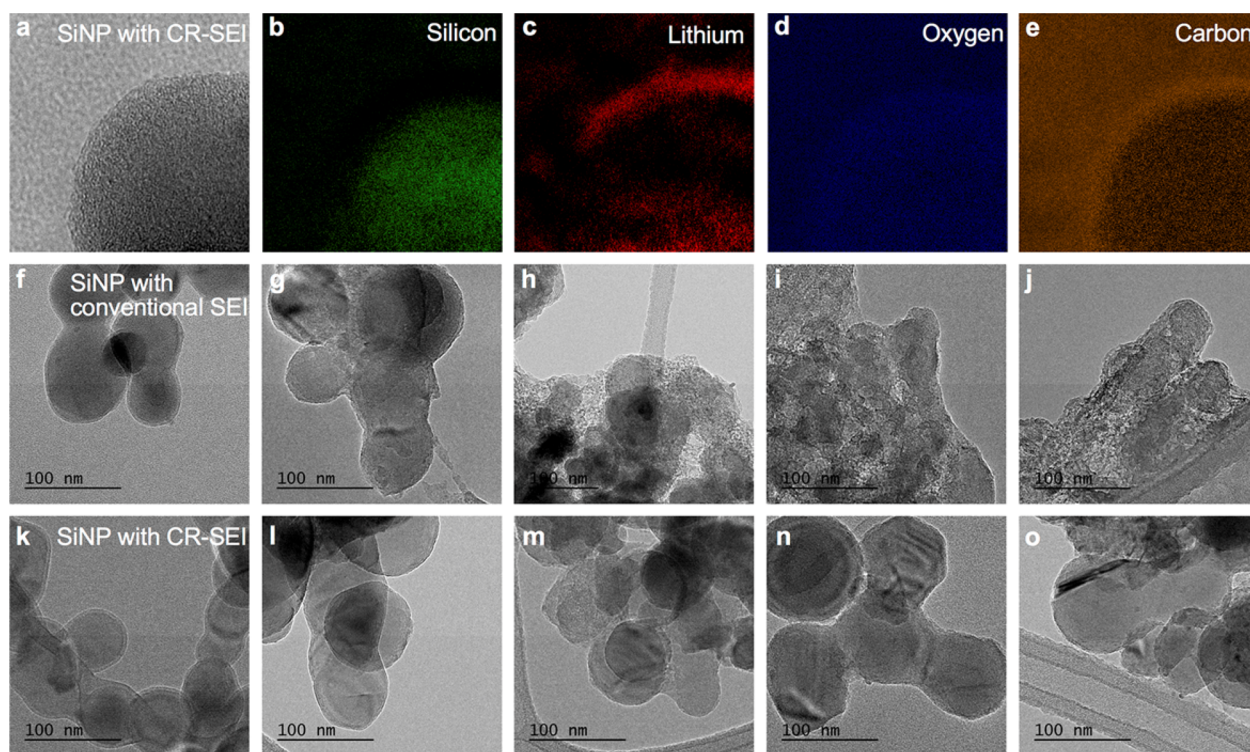


Figure 5. Morphological observation on a CR-SEI. (a–e) EF-TEM images of a SiNP with a CR-SEI display its thickness of about 10 nm and the uniform distribution of lithium (c), oxygen (d), and carbon (e) after 30 cycles. (f–j) TEM images of a SiNP with a conventional SEI: fresh Si (f), cycled Si after 1 cycle (g), 5 cycles (h), 50 cycles (i), and 100 cycles (j). The accumulation of “waste SEI” and the diminished SiNP imply the huge consumption of electrolyte and SiNP and the unstable conventional SEI. (k–o) TEM images of a SiNP with a CR-SEI: 3 (k), cycled Si after 1 cycle (l), 5 cycles (m), 50 cycles (n), and 100 cycles (o). Clear-edge SiNPs with retained size and limited electrolyte-decomposed products were captured after 50 and 100 cycles, evidencing the good stability of the CR-SEI. All samples were prepared at the delithiated status.

Particularly, the F concentration directly represents the LiPF_6 decomposition since LiPF_6 is the only F source. As shown in Figure 4c, the conventional SEI presents high Li and F concentrations, both of about 15% after one cycle, suggesting a severe decomposition of LiPF_6 and the formation of a large amount of Li salt species in the SEI. Their concentrations keep increasing to 25% after 100 cycles, while the C and O concentrations remain relatively low (both below 30%). In contrast, with the CR-SEI, the Li and F concentrations are 5.6% and 6.4% after one cycle and increase to 10.5% and 13.9% after 100 cycles, respectively, remaining at a low level. Meanwhile, the C and O concentrations are relatively high ($\sim 40\%$) and remain consistent during cycling (Figure 4d). The high concentration of organic oligomeric species in the CR-SEI represents the effective suppression of Li salt consumption, demonstrating a good stability of the CR-SEI. Additionally, the intensity of Si signal reflects the SEI thickness during cycling. The more strongly the Si signal is detected, the thinner the SEI is on the Si surface.⁴³ The pristine SiNP electrode surface before cycling contains 34.3% Si (Figure 4c), and the value for the uncycled SiNP electrode with 2–4 is 17.9% because of the presence of preanchored components and surface oxidation through the preparation process (Figure 4d). After one cycle, the apparent Si concentrations of the SiNP electrode with a conventional SEI and with a CR-SEI decrease to 3.3% and 7.0%, respectively, indicating that the electrode surfaces are both covered by the SEI. The Si concentration of the SiNP electrode with a conventional SEI further drops to 0.7% after five cycles, and the Si signal cannot be observed after 50 cycles, reflecting the formation of a large amount of “waste SEI”. In

contrast, the apparent Si surface concentrations of the SiNP electrode with CR-SEI are 5.4%, 2.1%, and 1.1% after the 5, 50, and 100 cycles, respectively. The long-lasting presence of the Si signal on the surface proves that CR-SEI remains thin and has very limited accumulation during cycling. To further verify the long-lasting anchoring of preanchored components within the SEI on the Si surface during cycling, we studied the cycled SiNP electrodes with the conventional SEI and CR-SEI after 100 cycles by XPS and TGA techniques after a thorough wash and ultrasonic treatment. No obvious carbonate-based species at 289.2 eV was detected by XPS measurements of the SiNP electrode with a conventional SEI, indicating that the conventional SEI components are removed (Figure 4e). In contrast, the characteristic peaks of 2 and 4 such as C–O (286.2 eV), oligomeric O–C=O (291.3 eV), and triazole (399.5 eV) were still observed on the Si with a CR-SEI surface, confirming the covalent bonding of preanchored SEI components to the SiNP surface after many cycles (Figure 4e). Meanwhile, TGA of the SiNP electrode with a CR-SEI after a wash and ultrasonic treatment shows an 8% weight loss below 450 °C, compared with the SiNP electrode with a conventional SEI. This finding also verifies the presence of the preanchored SEI components (Figure 4f).

Morphological Observations on the CR-SEI. To further demonstrate the stability of the CR-SEI, we next carried out morphological observations of the SEI during cycling. The thickness and elemental distribution of the CR-SEI were studied by energy-filtered transmission electron microscopy (EF-TEM). The CR-SEI after 30 cycles is less than 10 nm thick and uniformly coated on the SiNP surface (Figure 5a–e),

consistent with its good surface passivation and close contact with the Si surface. Furthermore, morphological changes in the CR-SEI during cycling were compared by TEM with those of the conventional SEI. Before cycling, fresh SiNPs with/without preanchored SEI components both show a perfectly round shape with a sharp edge (Figure S*k,f*). The preanchored SEI components are veiled under this length scale. After one cycle, the conventional SEI is rough and thick once formed. After five cycles, a large amount of “waste SEI” accumulation and a dramatic decrease in SiNP particle size were observed, indicating the severe consumption of electrolyte and SiNP material. No clear-edge SiNP particle can be recognized after 50 cycles (Figure S*g,h*). This result is in accord with the poor electrochemical performance and the high concentrations of Li and F of SiNP electrodes with the conventional SEI. In contrast, the thin SEI and clear-edge SiNPs of SiNP electrodes with a CR-SEI were observed after one, five, and 50 cycles. Only a small amount of “waste SEI” was found after 100 cycles, and the SiNP kept its round shape and size (Figure S*l–o*). In addition, thickness increases of the whole electrode can also imply the SEI accumulation. Based on the measurements of electrode thicknesses from scanning electron microscopy (SEM) images, the SiNP electrode with a CR-SEI presents a limited increase in electrode thickness compared to the SiNP electrode with the FEC-SEI during cycling, indicating the limited “waste SEI” accumulation (Figure S6). These observations confirm the significantly improved stability of the CR-SEI and are also consistent with results of the electrochemical and compositional analyses.

CONCLUSION

In summary, we present a new general strategy for deliberately controlling formation, composition, and morphology of the Li-alloy anodes SEI via covalently anchoring a combination of diverse functional components with precisely controlled structure and amount into the SEI using a one-step click chemistry. The CR-SEI presents improved tolerance to volume change, good surface passivation, and durable contact with the active material surface during cycling.

This concept has been demonstrated by the significantly improved stability of the SiNP anode SEI. By optimizing chemical structures, combinations, and surface anchoring amounts of the preanchored SEI components, we construct a CR-SEI, which exhibits a different chemical structure containing a high-concentration organic species, stable composition, and durable morphology during cycling. The CR-SEI enables greatly enhanced electrochemical performance of SiNP anodes, including long cycle life and high CE in both half and full cells, elevated first-cycle efficiency, and limited impedance increases during cycling. Moreover, this strategy has also been applied to GeNP SEI reinforcement with dramatic enhancement of the SEI stability, suggesting its viability for other Li-alloy materials.

Owing to the facility and modularity of click chemistry, this SEI reinforcement approach can be applied to other Li-alloy materials and more potential SEI components can be employed. This approach focuses on the interfacial construction of functional groups to construct a durable SEI. However, it is still unable to address the negative effects of pulverization on SEI stability of Li-alloy materials. Combining multiple approaches with this strategy shows promise in further improving SEI stability and enabling stable Li-alloy materials in LIBs.

EXPERIMENTAL SECTION

Synthesis of SiNP with Premodified SEI Components. The native oxide layer of SiNPs was removed by immersion in 5% HF in ethanol–water for 3 min under nitrogen. The product, hydrogen-terminated SiNPs (9), were washed with an ethanol–water mixture three times and dried in a vacuum oven. Then, dried 9 were mixed with propargyl ether and Karstedt catalyst, Platinum(0)-1,3-divinyl-1,1,3,3-tetramethyldisiloxane (Pt-dvs), in a molar ratio of 100:4 in anhydrous *N,N*-dimethylformamide (DMF) and heated at 170 °C with stirring for 4 h under nitrogen. The alkyne-terminated SiNPs (1) prepared in this way were rinsed with ethanol and toluene several times to remove unreacted residues and dried in a vacuum oven. To synthesize the SiNP with premodified SEI components, 1 was dispersed in aqueous solutions of azide-terminated components including 2', 3', 4', 5', combinations of 2' and 4', and combinations of 3' and 4' in designed molar ratios, and copper(II) sulfate pentahydrate and sodium ascorbate were added. This reaction was carried out at room temperature with stirring for 24 h under an air atmosphere.⁴⁷ The product was washed with deionized water and analytical grade ethanol three times and was dried in a vacuum oven for material characterization and electrode fabrication. GeNPs with 2–4 were synthesized similarly.

Electrode Fabrication and Electrochemical Testing. To compare the performance of the SiNP electrodes with a CR-SEI, FEC-SEI, and conventional SEI, we followed the same procedure to prepare SiNP electrodes and ran cell tests. SiNP electrodes were prepared by mixing pristine SiNPs/SiNPs with premodified SEI components, Super P carbon, and polyimide binder (7:2:1) in *N*-methylpyrrolidine to make a slurry, casting this slurry on a Cu foil, and drying it at 200 °C in a vacuum oven overnight. The mass loading of the electrode was about 1 mg/cm². Baseline electrolyte, which is 1 M LiPF₆ in a mixture of ethylene carbonate and ethyl methyl carbonate (3:7, v/v), was used to generate the conventional SEI and the conventional components in the CR-SEI. An FEC-derived SEI was formed from the baseline electrolyte containing 10% FEC additive. The electrolyte amount was controlled to 25 μL with a pipet. Electrochemical tests of cells were performed in CR 2016 coin cells under galvanostatic charging–discharging conditions at a C/3 rate (1C = 3000 mA/g Si) between 0.01 and 1.5 V. EIS testing was conducted with a Metrohm Autolab potentiostat (PGSTAT128N) between 0.1 and 100 000 Hz. The cells for the EIS test were held at 0.01 V for 30 min before testing. Full cell fabrication followed a preconditioning method.⁴¹ The SiNP anode was paired with a LiNi_{0.5}Co_{0.2}Mn_{0.3}O₂ cathode with a ratio of the areal capacity of 1.6. The SiNP anode was preconditioned for 10 cycles in the half-cell and terminated in the fully lithiated state while the LiNi_{0.5}Co_{0.2}Mn_{0.3}O₂ cathode was activated for three cycles in the half-cell, which ended at the fully delithiated state. Two precycled electrodes were paired as a coin-cell-type full cell. Cells were galvanostatically cycled at C/3 rate (1C = 3000 mA/g Si) from 3.0 to 4.2 V vs Li/Li⁺.

Materials and SEI Characterization. All samples for SEI analysis were tested once synthesized or achieved to prevent further oxidation or reactions. After disassembling the cell in an argon glovebox, electrode samples were rinsed and gently washed in diethylene carbonate (DEC) solution to remove salt and soluble species. XPS analysis was carried out on a PHI VersaProbe II scanning XPS microprobe. Air- and moisture-sensitive samples were loaded in the glovebox and transferred into the instrument through a vacuum transfer vessel. FTIR spectra were obtained on a Bruker Vertex V70 spectrometer. The electrode samples were tested in diffuse reflectance mode with a Spectra Tech Collector II cell filled with nitrogen. TGA was performed on a Q600 SDT using air flow with a balance sensitivity of 0.1 μg. Thirty mg SiNPs samples and 10 mg SiNP electrode samples were used for TGA tests, respectively. TEM samples were prepared by dispersing cycled SiNP electrodes in DEC and dripping them onto the TEM grid. EF-TEM and TEM images were acquired from a Tecnai G2 20 XTWIN with a LaB6 source. To remove electrochemically deposited SEI on the SiNP electrode surface, the electrodes were ultrasonically cleaned in DEC solution under a nitrogen atmosphere

for 3 h, washed with DEC three times, and then dried for XPS and TGA tests. Electrode thickness measurement was conducted on a Nova NanoSEM 630. To ensure the consistency of electrode thickness, the same piece of electrode was used for SEM experiments. ¹H NMR (400 Hz) spectra were recorded on a Bruker DRX 400 spectrometer.

■ ASSOCIATED CONTENT

Supporting Information

The Supporting Information is available free of charge on the ACS Publications website at DOI: 10.1021/jacs.7b07584.

Experimental details and additional characterizations (PDF)

■ AUTHOR INFORMATION

Corresponding Author

*dwang@engr.psu.edu

ORCID

Yue Gao: 0000-0001-7559-1288

Yuguang C. Li: 0000-0002-9559-7051

Thomas E. Mallouk: 0000-0003-4599-4208

Donghai Wang: 0000-0001-7261-8510

Notes

The authors declare no competing financial interest.

■ ACKNOWLEDGMENTS

This work was supported by the Assistant Secretary for Energy Efficiency and Renewable Energy, Office of Vehicle Technologies of the U.S. Department of Energy, under contract no. DE-EE0006447. Y.C.L. and T.E.M. acknowledge support from the National Science Foundation under grant DMR-1306938. We thank G. Chen and B. Wang from the Department of Chemistry at The Pennsylvania State University for providing facilities for organic synthesis. We also thank J. Gray from the Material Research Lab at The Pennsylvania State University for helping capture EF-TEM images.

■ REFERENCES

- Armand, M.; Tarascon, J.-M. *Nature* **2008**, *451*, 652.
- Goodenough, J. B.; Kim, Y. *Chem. Mater.* **2010**, *22*, 587.
- Tarascon, J. M.; Armand, M. *Nature* **2001**, *414*, 359.
- Park, C.-M.; Kim, J.-H.; Kim, H.; Sohn, H.-J. *Chem. Soc. Rev.* **2010**, *39*, 3115.
- Kiani, M. A.; Mousavi, M. F.; Rahmanifar, M. S. *Int. J. Electrochem. Sci.* **2011**, *6*, 2581.
- Sun, Y.; Liu, N.; Cui, Y. *Nat. Energy* **2016**, *1*, 16071.
- Su, X.; Wu, Q.; Li, J.; Xiao, X.; Lott, A.; Lu, W.; Sheldon, B. W.; Wu, J. *Adv. Energy Mater.* **2014**, *4*, 1300882.
- Wu, H.; Chan, G.; Choi, J. W.; Ryu, L.; Yao, Y.; McDowell, M. T.; Lee, S. W.; Jackson, A.; Yang, Y.; Hu, L.; Cui, Y. *Nat. Nanotechnol.* **2012**, *7*, 310.
- Liu, N.; Lu, Z.; Zhao, J.; McDowell, M. T.; Lee, H.-W.; Zhao, W.; Cui, Y. *Nat. Nanotechnol.* **2014**, *9*, 187.
- Magasinski, a; Dixon, P.; Hertzberg, B.; Kvit, A.; Ayala, J.; Yushin, G. *Nat. Mater.* **2010**, *9*, 353.
- Dai, F.; Zai, J.; Yi, R.; Gordin, M. L.; Sohn, H.; Chen, S.; Wang, D. *Nat. Commun.* **2014**, *5*, 3605.
- Yi, R.; Dai, F.; Gordin, M. L.; Chen, S.; Wang, D. *Adv. Energy Mater.* **2013**, *3*, 295.
- Li, X.; Gu, M.; Hu, S.; Kennard, R.; Yan, P.; Chen, X.; Wang, C.; Sailor, M. J.; Zhang, J.-G.; Liu, J. *Nat. Commun.* **2014**, *5*, 1.
- Ko, M.; Chae, S.; Ma, J.; Kim, N.; Lee, H.-W.; Cui, Y.; Cho, J. *Nat. Energy* **2016**, *1*, 16113.

- Derrien, G.; Hassoun, J.; Panero, S.; Scrosati, B. *Adv. Mater.* **2007**, *19*, 2336.
- Li, Y.; Yan, K.; Lee, H.-W.; Lu, Z.; Liu, N.; Cui, Y. *Nat. Energy* **2016**, *1*, 15029.
- Wang, C.; Wu, H.; Chen, Z.; McDowell, M. T.; Cui, Y.; Bao, Z. *Nat. Chem.* **2013**, *5*, 1042.
- Pan, L.; Yu, G.; Zhai, D.; Lee, H. R.; Zhao, W.; Liu, N.; Wang, H.; Tee, B. C.-K.; Shi, Y.; Cui, Y.; Bao, Z. *Proc. Natl. Acad. Sci. U. S. A.* **2012**, *109*, 9287.
- Aurbach, D. *J. Power Sources* **2000**, *89*, 206.
- Verma, P.; Maire, P.; Novák, P. *Electrochim. Acta* **2010**, *55*, 6332.
- Chan, C. K.; Ruffo, R.; Hong, S. S.; Cui, Y. *J. Power Sources* **2009**, *189*, 1132.
- Veith, G. M.; Doucet, M.; Baldwin, J. K.; Sacci, R. L.; Fears, T. M.; Wang, Y.; Browning, J. F. *J. Phys. Chem. C* **2015**, *119*, 20339.
- Horowitz, Y.; Han, H. L.; Ross, P. N.; Somorjai, G. A. *J. Am. Chem. Soc.* **2016**, *138*, 726.
- Michan, A. L.; Divitini, G.; Pell, A. J.; Leskes, M.; Ducati, C.; Grey, C. P. *J. Am. Chem. Soc.* **2016**, *138*, 7918.
- Zhan, C.; Lu, J.; Kropf, A. J.; Wu, T.; Jansen, A. N.; Sun, Y.-K.; Qiu, X.; Amine, K. *Nat. Commun.* **2013**, *4*, 2437.
- Busche, M. R.; Drossel, T.; Leichtweiss, T.; Weber, D. A.; Falk, M.; Schneider, M.; Reich, M.; Sommer, H.; Adelhelm, P.; Janek, J. *Nat. Chem.* **2016**, *8*, 1.
- Xu, K. *Chem. Rev.* **2014**, *114*, 11503.
- Li, J.; Dudney, N. J.; Nanda, J.; Liang, C. *ACS Appl. Mater. Interfaces* **2014**, *6*, 10083.
- Luo, L.; Yang, H.; Yan, P.; Travis, J. J.; Lee, Y.; Liu, N.; Molina Piper, D.; Lee, S. H.; Zhao, P.; George, S. M.; Zhang, J. G.; Cui, Y.; Zhang, S.; Ban, C.; Wang, C. M. *ACS Nano* **2015**, *9*, 5559.
- Xiao, X.; Lu, P.; Ahn, D. *Adv. Mater.* **2011**, *23*, 3911.
- Wu, H.; Yu, G.; Pan, L.; Liu, N.; McDowell, M. T.; Bao, Z.; Cui, Y. *Nat. Commun.* **2013**, *4*, 1943.
- Yao, Y.; Liu, N.; McDowell, M. T.; Pasta, M.; Cui, Y. *Energy Environ. Sci.* **2012**, *5*, 7927.
- He, Y.; Piper, D. M.; Gu, M.; Travis, J. J.; George, S. M.; Lee, S.-H.; Genc, A.; Pullan, L.; Liu, J.; Mao, S. X.; Zhang, J.-G.; Ban, C.; Wang, C. *ACS Nano* **2014**, *8*, 11816.
- Ng, S. H.; Wang, J.; Wexler, D.; Konstantinov, K.; Guo, Z. P.; Liu, H. K. *Angew. Chem., Int. Ed.* **2006**, *45*, 6896.
- Yi, R.; Dai, F.; Gordin, M. L.; Sohn, H.; Wang, D. *Adv. Energy Mater.* **2013**, *3*, 1507.
- Zhao, J.; Lu, Z.; Wang, H.; Liu, W.; Lee, H.-W.; Yan, K.; Zhuo, D.; Lin, D.; Liu, N.; Cui, Y. *J. Am. Chem. Soc.* **2015**, *137*, 8372.
- Min, J. H.; Bae, Y. S.; Kim, J. Y.; Kim, S. S.; Song, S. W. *Bull. Korean Chem. Soc.* **2013**, *34*, 1296.
- Xu, W.; Vegunta, S. S. S.; Flake, J. C. *J. Power Sources* **2011**, *196*, 8583.
- Dalavi, S.; Guduru, P.; Lucht, B. L. *J. Electrochem. Soc.* **2012**, *159*, A642.
- Philippe, B.; Dedryveire, R.; Gorgoi, M.; Rensmo, H.; Gonbeau, D.; Edström, K. *J. Am. Chem. Soc.* **2013**, *135*, 9829.
- Piper, D. M.; Evans, T.; Leung, K.; Watkins, T.; Olson, J.; Kim, S. C.; Han, S. S.; Bhat, V.; Oh, K. H.; Buttry, D. a; Lee, S.-H. *Nat. Commun.* **2015**, *6*, 1.
- Zhang, S. S. *J. Power Sources* **2006**, *162*, 1379.
- Nakai, H.; Kubota, T.; Kita, A.; Kawashima, A. *J. Electrochem. Soc.* **2011**, *158*, A798.
- Aurbach, D.; Gamolsky, K.; Markovsky, B.; Gofer, Y.; Schmidt, M.; Heider, U. *Electrochim. Acta* **2002**, *47*, 1423.
- Etacheri, V.; Haik, O.; Goffer, Y.; Roberts, G. A.; Stefan, I. C.; Fasching, R.; Aurbach, D. *Langmuir* **2012**, *28*, 965.
- Nandivada, H.; Jiang, X.; Lahann, J. *Adv. Mater.* **2007**, *19*, 2197.
- Ciampi, S.; Böcking, T.; Kilian, K. A.; James, M.; Harper, J. B.; Gooding, J. J. *Langmuir* **2007**, *23*, 9320.
- Ota, H.; Sakata, Y.; Inoue, A.; Yamaguchi, S. *J. Electrochem. Soc.* **2004**, *151*, A1659.
- Chen, L.; Wang, K.; Xie, X.; Xie, J. *J. Power Sources* **2007**, *174*, 538.

(50) Schroder, K. W.; Celio, H.; Webb, L. J.; Stevenson, K. J. *J. Phys. Chem. C* **2012**, *116*, 19737.